Charge Photogeneration in Few-Layer MoS_2

Tetiana Borzda, Christoph Gadermaier,* Natasa Vujicic, Peter Topolovsek, Milos Borovsak, Tomaz Mertelj, Daniele Viola, Cristian Manzoni, Eva A. A. Pogna, Daniele Brida, Maria Rosa Antognazza, Francesco Scotognella, Guglielmo Lanzani, Giulio Cerullo, and Dragan Mihailovic*

The 2D semiconductor MoS_2 in its mono- and few-layer form is expected to have a significant exciton binding energy of several 100 meV, suggesting excitons as the primary photoexcited species. Nevertheless, even single layers show a strong photovoltaic effect and work as the active material in high sensitivity photodetectors, thus indicating efficient charge carrier photogeneration. Here, modulation spectroscopy in the sub-ps and ms time scales is used to study the photoexcitation dynamics in few-layer MoS_2. The results suggest that the primary photoexcitations are excitons that efficiently dissociate into charges with a characteristic time of 700 fs. Based on these findings, simple suggestions for the design of efficient MoS_2 photovoltaic and photodetector devices are made.

1. Introduction

Recent progress in the exfoliation of layered materials[1,2] and the nanofabrication of functional structures has revived the interest in 2D materials with properties complementary to graphene, in particular transition metal dichalcogenides[3,4] (TMDs) such as MoS_2. Depending on the metal atoms' coordination and oxidation state, TMDs can be metallic, semimetallic, or semiconducting. In addition, some TMDs show superconductivity,[5] charge-density waves,[6] and hidden electronically ordered phases.[7] Their potential for electronics has become evident by the realization of a field-effect transistor[8] (FET) and a logic circuit device[9] based on a single flake of monolayer MoS_2.

The optical absorption of MoS_2 in the visible spectral range shows four excitonic resonances,[10] commonly labeled (see **Figure 1**a) A to D at 1.9, 2.1, 2.7, and 2.9 eV. The spectral positions of these resonances are almost independent of the number of layers, whereas the indirect band gap is at 1.2 eV in the bulk and grows progressively as the number of layers is reduced, even exceeding the energy of the A exciton resonance for the monolayer. Hence, the monolayer, contrary to bi- and multilayers, behaves like a direct gap semiconductor and shows significant fluorescence.[11,12] The exciton binding energy for bulk MoS_2 has been determined to be 45 and 130 meV for the A and B excitons, respectively.[13] Both exciton binding energies increase upon decreasing the sample thickness, with estimates for monolayer[14–16] ranging from 0.4 to 0.9 eV. Despite this high exciton binding energy, monolayer MoS_2 shows a strong photovoltaic effect[17] and potential for high sensitivity photodetectors.[18] Both these functionalities require efficient charge carrier photogeneration (CPG), either via direct excitation of mobile carriers or via exciton dissociation.

The spectral signature of charge carriers has been identified by absorption and fluorescence spectroscopy of MoS_2, where the charge concentration varies either via the gate voltage in an FET geometry[19] or via adsorption,[20] or substrate doping.[21] The absorption peaks of charges are red-shifted by about 40 meV compared with the ground-state absorption into the A and B excitons and have been attributed to optical transitions from a charged ground state to a charged exciton (trion). The possibility of alternative interpretations, such as polarons[22,23] or Stark effect in the local electric field of the charges,[24–26] does

T. Borzda, Prof. C. Gadermaier, Dr. N. Vujicic, P. Topolovsek, M. Borovsak, Dr. T. Mertelj, Prof. D. Mihailovic
Department of Complex Matter
Jozef Stefan Institute
Jamova 39, 1000 Ljubljana, Slovenia
E-mail: tetiana.borzda@ijs.si; christoph.gadermaier@ijs.si

T. Borzda, Prof. C. Gadermaier, P. Topolovsek, Prof. D. Mihailovic
Jozef Stefan International Postgraduate School
Jamova 39, 1000 Ljubljana, Slovenia

Dr. N. Vujicic
Institute of Physics
Bijenicka 46, 10000 Zagreb, Croatia

M. Borovsak
Faculty of Mathematics and Physics
University of Ljubljana
Jadranska 19, 1000 Ljubljana, Slovenia

D. Viola, Dr. C. Manzoni, E. A. A. Pogna, Dr. F. Scotognella, Prof. G. Lanzani, Prof. G. Cerullo
IFN-CNR, Department of Physics
Politecnico di Milano
P. Leonardo da Vinci 32, 20133 Milan, Italy

Dr. D. Brida
Department of Physics and Center of Applied Photonics
University of Konstanz
D-78457 Konstanz, Germany

Dr. M. R. Antognazza, Dr. F. Scotognella, Prof. G. Lanzani
Center for Nano Science and Technology
Italian Institute of Technology
Via Pascoli 70/3, 20133 Milano, Italy

Prof. D. Mihailovic
Center of Excellence in Nanoscience and Nanotechnology
Jamova 39, 1000 Ljubljana, Slovenia

DOI: 10.1002/adfm.201500709

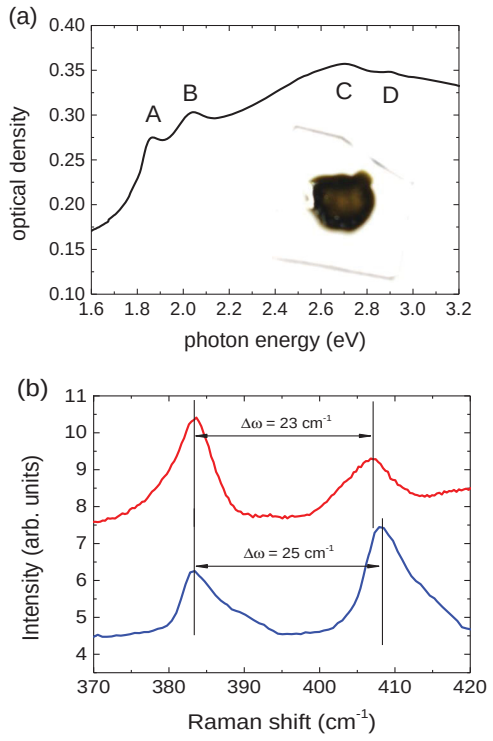

Figure 1. a) Absorption spectrum of the sample of MoS_2 in PMMA. The inset shows a photograph (the dark area has a diameter of approximately 7–8 mm). b) Raman spectra for two excitation wavelengths at 633 nm (red line) and 488 nm (blue line).

not compromise the identification of these absorption peaks as belonging to charges.

Here, we use continuous wave (cw) photomodulation (PM) and femtosecond pump–probe spectroscopy to identify the spectral features of photogenerated charges and trace their dynamics, starting with their generation either by direct impulsive excitation into the charge continuum or via exciton dissociation. We exfoliated MoS_2 in ethanol, following the protocol in ref. [1]. The dispersion was dried and the obtained few-layer flakes were re-dispersed in a solution of poly(methyl methacrylate) (PMMA), a transparent and electronically inert polymer. This dispersion was spin-cast onto a quartz substrate, yielding a macroscopic PMMA film with a homogenous greenish-yellow color characteristic of thin MoS_2 films[27] (see Figure 1a). PMMA, in this sample, serves as a matrix that holds an ensemble of flakes with lateral size[1] of few-hundred nanometers. More details about the sample preparation are found in the Methods section. The distance $\Delta\omega$ between the two Raman peaks around 400 cm^{-1} is generally viewed as the most robust measure of the flake thickness.[28] From the Raman spectra in Figure 1b, we obtain $\Delta\omega$ = 23 cm^{-1} for excitation at 633 nm and $\Delta\omega$ = 25 cm^{-1} at 488 nm. Within the distribution, various thicknesses contribute differently to the two excitation wavelengths.[29] Overall, the Raman spectra indicate a flake thickness distribution that is dominated by three- to six-layer flakes.

The advantages of this kind of sample compared with individual flakes are the ease of fabrication and handling and the possibility of using any spectroscopic technique without the need for high-resolution optical microscopy. MoS_2 flakes embedded in PMMA are in a slightly different environment than mono- or few-layer flakes on dielectric substrates used in previous femtosecond studies.[30,31] However, as our results will show, the spectra and the relaxation times of the signal are very similar to those obtained on individual few-layer flakes. Hence, the present study directly extends existing knowledge on the femtosecond behavior of few-layer MoS_2.

2. Results and Discussion

The absorption spectrum in Figure 1a shows the characteristic A and B exciton resonances, which are broader and red-shifted compared with undoped MoS_2, as is typical of commercial MoS_2 of mineral origin,[32] which is doped due to dislocations induced by the exfoliation and due to (mostly metallic) impurities. Hence, each of the two absorption peaks is actually an overlap of at least two contributions: neutral ground state to exciton absorption at the higher energy side of each peak and lowest charged state to excited charged state at the lower energy side. For the A peak, an even lower energy contribution has been identified,[32] which has alternatively been ascribed to a surface-trapped exciton,[33] an edge state,[34] or a plasmon resonance,[35] so that peak A actually arises from the overlap of three peaks. Similar to the notation in refs. [19,20,32], we will use the labels L, A^-, and A^0 for the low energy peak, charge peak, and exciton peak of the A resonance, and B^- and B^0 for the charged and neutral contributions to the B resonance. Please note that, contrary to electrical or chemical doping, photoexcitation generates charges in pairs of opposite polarities. However, although we expect the signatures of the corresponding positive charges at the same spectral positions, we know only those of the negative charges, hence our labeling.

To identify long-lived photoexcitations we performed cw PM spectroscopy. Here, a cw laser with 3.1 eV photon energy used for exciting the sample is periodically modulated via a mechanical chopper. The relative change $\Delta T/T$ of the transmitted light from a halogen lamp is measured via phase-sensitive detection (see the Experimental Section for details). Those photoexcitations whose population changes significantly over the modulation cycle (i.e., their lifetime is long enough to build up sufficient population while the laser is on and short enough to sufficiently reduce their population while it is off) are identified in the cw PM spectrum via their photoinduced absorption (negative $\Delta T/T$) transitions to higher excited states. Concomitantly with the increase of photoexcited populations, the ground-state population and its associated absorption are reduced (photobleaching, positive $\Delta T/T$). The cw PM spectrum at room temperature upon excitation at 3.1 eV, above the C and D exciton resonances, is shown in **Figure 2**a. The signal is largely in phase with the modulation of the photoexcitation, with a negligible quadrature contribution. This means that the populations at the origin of the signal can easily follow the modulation at 245 Hz, implying that the lifetimes of the respective photogenerated species are much shorter than the modulation period of ≈4 ms. The main features of the spectrum are three positive (photobleaching) and two negative (photoinduced absorption) peaks. We fit the spectrum using five overlapping Gaussians (see Figure 2b), which represent the thermal and

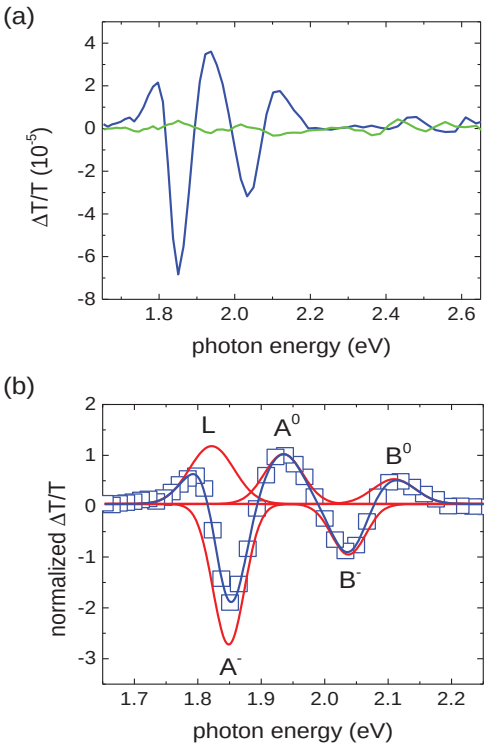

Figure 2. a) cw photoinduced absorption spectrum of MoS_2 in PMMA at room temperature for excitation at 3.1 eV. In-phase (blue) and quadrature (green) signal components are shown for a modulation frequency of 245 Hz. b) Five Gaussian fits (red) whose sum (blue) fits the normalized in-phase spectrum (open squares).

disorder-induced (in particular by polydispersity of flake thickness) broadening of the electronic resonances. The strong overlap between neighboring peaks makes them appear narrower than their actual lineshape and connected by an almost straight line, masking the inflection points characteristic of isolated Gaussian peaks. The spectral positions of the five peaks correspond very well with the three neutral and two charge peaks discussed in refs. [19,20,32] Assuming the same origin for the peaks in the PM spectrum, we obtain a straightforward interpretation. Upon photoexcitation, the number of electrons in the neutral ground state is reduced, and the number of charge carriers is increased. Hence, the absorption features L, A^0, and B^0 from transitions between neutral states are reduced, resulting in a positive $\Delta T/T$ (photobleaching), while the absorption features A^- and B^- from charges are increased, yielding a negative $\Delta T/T$ (photoinduced absorption).

Alternatively, one could interpret the PM spectrum based on its resemblance of a derivative lineshape. A photoinduced blue shift of the absorption spectrum would result in a $\Delta T/T$ contribution that follows the first derivative of the absorption spectrum (or a negative first derivative for a red-shift); a photoinduced broadening of the absorption peaks would contribute a negative second derivative. If we interpreted our spectrum in terms of derivative lineshapes, it would be dominated by a positive second derivative, which indicates a photoinduced line narrowing. We are not aware of any such mechanism. However, the A peak is composed of the three overlapping narrower peaks L, A^-, and A^0 (no equivalent to the L peak has yet been identified for the B peak, but we may extrapolate our reasoning also to B). In our proposed scenario, photoexcitation generates charges and the middle peak A^- increases at the expense of the other two, which decreases the overall width of the A peak. Hence, CPG leads to an apparent photoinduced line narrowing, which explains the positive second derivative lineshape.

To investigate CPG in real time, we employed femtosecond optical pump–probe spectroscopy. Like cw PM, this technique measures the relative change in transmission $\Delta T/T$. However, rather than continuously, the sample is photoexcited impulsively at a well-defined point in time by an fs laser pulse (the pump) and the transient transmission spectrum is measured with a second fs laser pulse (the probe) at a well-defined delay after the pump. Scanning the pump–probe delay allows following the evolution of the photoexcited states' populations (see details in the Experimental section). We start by comparing the $\Delta T/T$ signal for excitation at 3.1 eV at long pump–probe delay (300 ps) with the cw PM (see **Figure 3**a). The two normalized spectra are very similar, with three important differences: in the fs transient spectrum the L peak is absent, there is an additional broad photoinduced absorption feature peaking around 2.45 eV, and the whole spectrum is red-shifted. This red-shift is more pronounced at higher pump intensities (see Figure 3b) and shorter pump–probe delays (see Figure 3c,d). Both these correlations suggest that the red-shift is stronger for higher concentration of a certain species of excited states. The most intuitive interpretations are Stark effect due to the local field of photogenerated charges, as has been observed in semiconductor nanocrystals,[24] organic semiconductors,[25] and carbon nanotubes,[26,36] inter-excitonic interaction,[37] or band gap renormalization, as has been found in semiconducting quantum wells upon photoexcitation[38] and inferred in recent works on semiconducting TMDs.[39,40] This intensity-dependent red-shift also explains how the nonlinear optical properties of MoS_2 can change from saturable absorption (i.e., photobleaching) to optical limiting (i.e., photoinduced absorption) as a function of pump intensity.[41] After approximately 3 ps, the spectrum decays without any significant shifts or changes of shape, through a dominant process with a time constant of approximately 500 ps (see Figure 3e), as previously obtained on few-layer MoS_2 supported on a dielectric substrate.[30]

In addition to the previously identified A^-, A^0, B^-, and B^0 peaks, we note an additional broad absorption peak and a further positive peak at higher probe energies. Due to its position, we straightforwardly assign the positive peak to bleaching of the C exciton and label it C^0. The absorption peak shows a formation similar to A^- and B^- (see the next paragraph), and is similarly long lived; hence, it should belong to a charge population. Like the C exciton bleaching, it is absent in cw PM and strongly reduced for excitation energies below the C exciton resonance (see Figure 3f); hence, we ascribe it to a charge associated with the C exciton, labeled C^-. The C exciton is ascribed either to excitation from a band below the valence band, or between the valence and conduction bands in a region of the bands nesting slightly off the Γ point.[42] In both scenarios, it is plausible that the C^0 and C^- features do not appear in the cw experiment, which probes populations that have relaxed toward the edges of the band gap.

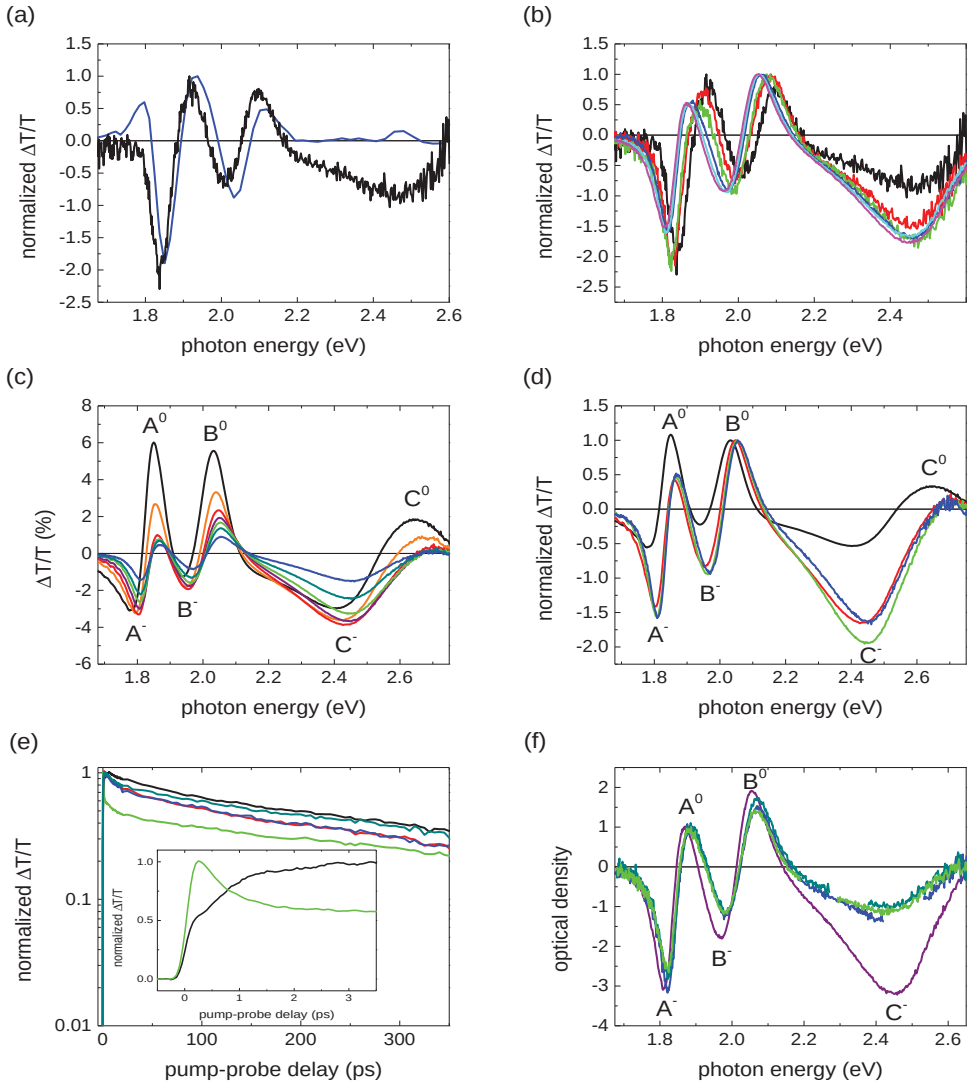

Figure 3. a) Normalized cw photomodulation spectrum of MoS_2 in PMMA (blue) compared with the fs transient spectrum at 300 ps pump–probe (black) delay for 2×10^{14} cm^{-2} excitation fluence, 3.1 eV pump photon energy. b) Pump–probe spectra at 300 ps normalized to the B exciton peak for different pump fluences at 3.1 eV pump photon energy: 2 (black), 3 (red), 6 (green), 20 (blue), 40 (cyan), and 80×10^{14} cm^{-2} (magenta). c) Absolute and pump–probe spectra for 4×10^{15} cm^{-2} pump fluence at delays 300 fs (black), 1 ps (orange), 3 ps (red), 10 ps (purple), 30 ps (green), 100 ps (dark cyan), and 300 ps (blue). d) Selected spectra from (c) normalized to the B^0 peak. e) Normalized time traces for different probe energies: 2.48 (black), 2.25 (red), 2.07 (green), 1.94 (blue), and 1.80 eV (dark cyan). f) Normalized spectra at 300 ps pump–probe delay for different pump photon energies: 3.10 (purple), 2.48 (blue), 2.34 (dark cyan), and 2.25 eV (green).

During the first 3 ps the $\Delta T/T$ spectrum undergoes a characteristic change of shape; the positive signal components are formed during the instrumental resolution and decay monotonically, while the main photoinduced absorption features, associated with charges A^-, B^-, and C^-, show an initial instrument-limited rise followed by a delayed rise component after the pump pulse and by a slower decay (see Figure 3e, inset). The simplest scenario of the underlying photoexcitation dynamics that is consistent with these results is sketched in **Figure 4**a. The pump pulse generates excitons as the primary photoexcited species, and these excitons dissociate into pairs of charges with a characteristic time τ_1

$$\frac{dE(t)}{dt} = G(t) - k_1 E(t) \tag{1a}$$

$$\frac{dC(t)}{dt} = k_1 E(t) - k_2 C(t) \tag{1b}$$

with E and C being the time-dependent overall exciton (A^0, B^0, and C^0) and charge (A^-, B^-, and C^-) populations and $G(t)$ the exciton generation term (pump–probe cross-correlation, approximated as a Gaussian). $k_1 = 1/\tau_1$ is the rate constant of exciton dissociation and $k_2 = 1/\tau_2$ is the rate constant of charge recombination. The evolution of the photoexcited states' population according to Equations (1a) and (1b) is best fitted

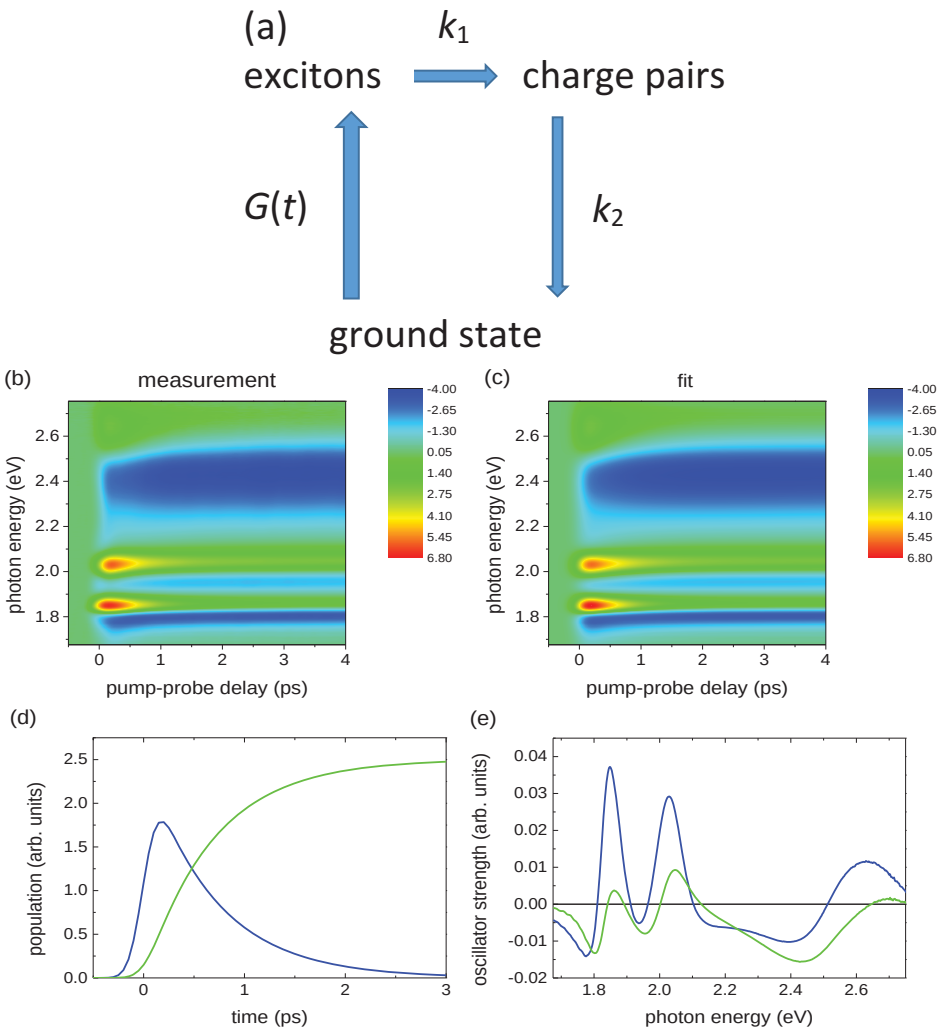

Figure 4. a) Scheme of the photoexcitation dynamics of excitons and charges. b) Contour plot of the measured $\Delta T/T$ (in %). c) Contour plot of the fitted $\Delta T/T$ (in %). d) Time-dependent exciton (blue) and charge (green) populations. e) Spectral contributions of excitons (blue) and charges (green).

with a characteristic time $\tau_1 = 700$ fs. The assumption of only one common time constant τ_1 for the dissociation of A, B, and C excitons may be a strong simplification, but it describes the data remarkably well (Figure 4b,c).

The time-dependent exciton and charge populations and their contributions to the $\Delta T/T$ signal are shown in Figure 4d,e, respectively. Please note that exciton dissociation already occurs during the pump pulse; therefore, at all times the exciton population is lower than the number of absorbed photons and lower than the number of charge pairs that are eventually created. The spectral contributions, given as oscillator strength in arbitrary units, include both the photoinduced absorption features of excitons and charges (shown as negative oscillator strength in Figure 4e) and their contribution to the bleaching (as positive oscillator strength). The bleaching contribution of charges is significantly smaller than that of excitons, suggesting that charges are more localized than excitons.[43]

The exciton spectrum in Figure 4e contains, in addition to the three well-known bleaching peaks, also several photoinduced absorption features. It is common in excitonic materials to observe such absorptions due to transitions from the lowest exciton level toward an exciton that involves an electron in a band higher than the conduction band (CB) or a hole below the valence band (VB).[44,45] The band structure of MoS_2 has many such bands,[14,15] and in particular at the K point, where the direct exciton is located, there are several band maxima and minima within the relevant range of 1–3 eV above the CB and below the VB, which can get involved in higher excitons A^* or B^*. While a precise identification of which bands are involved would require a detailed quantum chemical calculation of the transition matrix elements, which is beyond the scope of this paper, we can generally assign the photoinduced absorption peaks of the exciton population to transitions A^0–A^* or B^0–B^*.

Compared with our simplest scenario for the photoexcitation dynamics, two additional effects deserve consideration: direct excitation of charges and incomplete dissociation of the exciton population. In the Supporting Information, we examine in detail how the exciton and charge spectra change if we include these effects. In summary, while neither of the two effects can

be excluded a priori, for both of them the spectra become less plausible, the stronger we assume their contribution to the photoexcitation dynamics. This confirms that the simplest possible scenario, as given in Figure 4a, adequately describes our experimental results.

While for excitation at 3.1 eV our results suggest that all photoexcited excitons eventually dissociate with a characteristic time of 700 fs, Figure 3f shows that the ratio between the absorption peaks due to charges and the respective bleaching peaks is slightly lower for lower excitation energy. This finding suggests that for lower pump photon energies, the charge yield can be somewhat lower than 100%. An analogous result has been published for an MoS_2 monolayer, where the lower photoluminescence quantum yield for higher excitation energy has also been ascribed to stronger exciton dissociation.[42]

Let us now put our findings into context by comparing them to high-exciton binding energy materials on the one hand, and conventional semiconductors on the other hand. Detailed studies of the CPG dynamics exist for carbon nanotubes and conjugated polymers, whose exciton binding energies are similar to bilayer MoS_2, which is somewhat higher than in our samples. In carbon nanotubes, there is an initial branching between mostly excitons and 1%–2% directly excited charges,[36] with a higher charge yield for higher excitation energy. In conjugated polymers, there is a similar initial branching, followed by additional CPG via dissociation of "hot" excitons during the first few picoseconds.[46] Elaborate models describe how the surplus energy of hot excitons increases their dissociation probability.[47,48] The relaxation of the electron and hole to the lowest exciton state are typically faster than our observed 700 fs;[49–51] however, electron–phonon coupling creates a phonon heat bath that can live on for a few picoseconds.[52] In addition, exciton migration, which is facilitated by the excess energy and comes to a halt when the exciton reaches a local energy minimum, increases the probability that the exciton reaches a site where its dissociation is facilitated. In MoS_2 flakes, such sites could be surface defects, flake edges, metallic inclusions, crystal faults, or small islands of an extra MoS_2 layer. In the few-layer flakes of our study, for excitation at 3.1 eV, the exciton dissociation yield is close to 100% and only slightly lower for lower pump energies above the B exciton resonance. Hence, if hot exciton dissociation (phonon- or defect-mediated) mechanisms play a role, they are masked by the already high dissociation yield observed just above the B exciton resonance.

In conventional bulk semiconductors, the exciton binding energy is typically so low that at room temperature free carriers are photoexcited directly, prevalently across the direct gap. In the case of indirect gap semiconductors, the photoexcited electrons and holes relax toward the CB minimum and VB maximum of the indirect gap on a time scale of 100–200 fs.[49,53] This fast relaxation is the reason for the low fluorescence quantum yield of indirect semiconductors. In our case, the exciton binding energy is sufficient to have excitons as the primary photoexcited species, but is insufficient to prevent their subsequent dissociation. The relaxation toward the indirect gap is possible only if it is preceded or accompanied by exciton dissociation, which is the rate-limiting step in this case. An exciton lifetime of 700 fs is still much shorter than the 60 ps observed at room temperature for the monolayer[54] and can hence explain the much lower quantum yield of the excitonic fluorescence in the few-layer case.[11] For a bilayer of WSe_2 at 4 K the direct gap fluorescence bears a lifetime of 3 ps, while the indirect gap fluorescence has an onset that is delayed by a few picoseconds.[55] We can hence assume an analogous mechanism as we observe in the few-layer MoS_2 flakes, where exciton dissociation enables the carriers to scatter toward the indirect gap. Due to the higher exciton binding energy in the bilayer, the exciton dissociation and hence the scattering toward the indirect gap is slower than in our case.

Before we discuss the implications of efficient exciton dissociation, we review how our findings compare to previous femtosecond work on TMDs. Intervalley scattering[56,57] requires circular polarization and is not probed in our experiment, because all our laser polarizations are linear. On a time scale of 1–500 ps, Shi et al.[30] obtained results very similar to ours in few-layer flakes deposited on a dielectric substrate, but they do not discuss the temporal change of shape of the spectrum, which is crucial to understanding exciton dissociation and charge generation. They estimate that for excitation fluences similar to ours, the sample temperature should change by only 0.1 K, thus dismissing sample heating as a possible source of the signal. In our samples, due to the low heat conductivity of PMMA,[58] heating could be a bit stronger. However, a signal due to heating would not change its shape with time and, most crucially, at least for comparable absorbed fluences, its shape would not depend on the excitation photon energy. In Figure 3f, there is a small C^- signal even for excitation below the C exciton resonance. This contribution, which at any delay is 20% or less compared with the spectrum for excitation above the C resonance, may originate from heating or any other mechanism that changes the overall lineshapes and/or peak positions, such as Stark effect or band gap renormalization. Hence, for the combination of all such processes including heating, we estimate an upper boundary of 20% contribution to the transient signal. Any such mechanism is less important in the cw PM experiment, where no appreciable C^- signal is found. Therefore, both the femtosecond and the cw signals are dominated by changes in excited and ground-state populations, not pure lineshape/shift mechanisms.

Considering further lineshape/shift mechanisms, inter-exciton interaction is expected to result in a red-shift[37] and line broadening. However, we observe an apparent line narrowing (see the discussion of the cw PM spectrum) due to the increase of the central A^- peak at the expense of its neighbors on either side. The Burstein–Moss effect, which has been observed in substitutionally doped MoS_2 fullerenes,[59] should lead to a blue shift with increasing excited-state population. Our contrasting observation implies that any Burstein–Moss contribution is overwhelmed by one or more red-shifting mechanisms.

3. Conclusion

We have developed a scenario of the exciton and charge dynamics in few-layer MoS_2 where femtosecond pump–probe results are best described, assuming that the primary photoexcitations are excitons that dissociate efficiently with a characteristic time of 700 fs. Thus, few-layer MoS_2 displays a behavior

that is intermediate between conventional semiconductors on one hand, and high exciton binding energy materials, such as organic semiconductors, carbon nanotubes, and presumably single-layer MoS_2 on the other hand. Our results suggest that few-layer MoS_2 flakes can be employed in high-efficiency photodetectors and photovoltaic elements. Such devices have been shown based on monolayer field-effect transistors.[17,18] However, due to the higher exciton binding energy, in the monolayer the CPG yield is expected to be significantly lower. This assumption is corroborated by the observation that measures that facilitate exciton dissociation have strongly improved the efficiency of such devices. Such measures include a strong built-in field using appropriate electrode materials, by engineering a p–n junction,[60,61] or by combining MoS_2 with a second material,[62–64] so that one of them acts as an electron donor and the other as an acceptor in a heterojunction. According to our findings, in few-layers, which have the added benefit of absorbing a larger fraction of the incident light, such measures should not be necessary and simpler, more scalable device structures could be used.

4. Experimental Section

MoS_2 Sample Preparation: 1 mg of MoS_2 in water/ethanol mixture (Graphene Supermarket) was extracted by flocculation with the addition of KCl (potassium chloride ≥99.0 %, Sigma) into a solution. Obtained flocculates were repeatedly washed with a fresh water/ethanol (1:1) mixture to remove any salt residues. Solvent mixture of water and ethanol was then replaced by the absolute ethanol only. Sedimented MoS_2 was extracted from the bottom with a minimum amount of solvent and redispersed in 2 mL of chlorobenzene in an ultrasonic bath. 40 mg of PMMA (poly(methyl methacrylate) avg. $M_W \approx 350\,000$, Aldrich) was added to a solution of MoS_2 and sonicated at 50 °C for 30 min. 30 µL of the obtained stable solution was drop-cast onto a quartz substrate and left to dry in air. All spectroscopic investigations were performed at room temperature. Raman spectroscopic characterization of MoS_2 was performed with an NT-MDT NTEGRA SPECTRA confocal Raman microscope in backscattering geometry with spectral resolution of 0.7 cm^{-1}. We used the excitation lines at 488 nm (Argon ion laser) and 632.8 nm (He–Ne laser) and a 100× objective (NA 0.9) to focus onto a spot size of 3 µm. The Raman signals were detected with a CCD array at −70 °C. We used a laser power below 3 mW to avoid damaging the sample. The probe used in the cw PM experiment is a halogen lamp (ASB-W-30 from Spectral Products) filtered by a monochromator (CM 112 from Spectral Products with 0.3 mm slits). Excitation is provided by a diode laser at 405 nm (3.1 eV) with a power of 85 mW, focused on a spot of 8 mm diameter, mechanically modulated by a chopper (MC 1000A Optical Chopper System from Thorlabs).

Ultrafast Spectroscopy: The femtosecond pump–probe spectroscopy setup is driven by an amplified Ti:sapphire laser (Coherent Libra) producing 4 mJ, 100 fs, 1.55 eV pulses at 1 kHz repetition rate. A fraction of the pulse energy is used to drive a second-harmonic (SH) pumped optical parametric amplifier (OPA), generating ≈70 fs pulses tunable from 1.65 to 2.5 eV; the pump pulses are provided either by the OPA or by the SH of Ti:sapphire. Another fraction of the pulse energy is focused in a 3 mm thick sapphire plate to generate a single-filament white light continuum used as a probe. Pump and probe are noncollinearly focused on the sample, and the transmitted probe spectrum is detected by a spectrometer working at the full 1 kHz repetition rate of the laser. $\Delta T/T$ spectra are recorded with a time resolution of ≈100 fs and a sensitivity of 10^{-5}.

Supporting Information

Supporting Information is available from the Wiley Online Library or from the author.

Acknowledgements

The authors appreciate the stimulating discussions with V. Kabanov, L. Lüer, I. Madan, D. Polli, J. Rehault, G. Seifert, A. Shumilin, J. Strle, and R. Tenne. The research leading to these results has received funding from LASERLAB-EUROPE (Grant Agreement No. 284464, EC's Seventh Framework Programme), Zukunftskolleg, the Marie Curie CIG project "UltraQuEsT" No. 334463, the ERC Advanced Grant "Trajectory," and the Graphene Flagship (Contract No. CNECT-ICT-604391). The research was carried out in the context of the Marie-Curie ITN "MoWSeS" and the COST "Nanospectroscopy."

Received: February 20, 2015
Published online: April 28, 2015

[1] J. N. Coleman, M. Lotya, A. O'Neill, S. D. Bergin, P. J. King, U. Khan, K. Young, A. Gaucher, S. De, R. J. Smith, I. V. Shvets, S. K. Arora, G. Stanton, H.-Y. Kim, K. Lee, G. Tae Kim, G. S. Duesberg, T. Hallam, J. J. Boland, J. J. Wang, J. F. Donegan, J. C. Grunlan, G. Moriarty, A. Shmeliov, R. J. Nicholls, J. M. Perkins, E. M. Grieveson, K. Theuwissen, D. W. McComb, P. D. Nellist, V. Nicolosi, *Science* **2011**, *331*, 568.
[2] V. Nicolosi, M. Chhowalla, M. G. Kanatzidis, M. S. Strano, J. N. Coleman, *Science* **2013**, *340*, 1420.
[3] Q. H. Wang, K. Kalantar-Zadeh, A. Kis, J. N. Coleman, M. S. Strano, *Nat. Nanotechnol.* **2012**, *7*, 699.
[4] S. Z. Butler, S. M. Hollen, L. Cao, Y. Cui, J. A. Gupta, H. R. Gutiérrez, T. F. Heinz, S. S. Hong, J. Huang, A. F. Ismach, E. Johnston-Halperin, M. Kuno, V. V. Plashnitsa, R. D. Robinson, R. S. Ruoff, S. Salahuddin, J. Shan, L. Shi, M. G. Spencer, M. Terrones, W. Windl, J. E. Goldberger, *ACS Nano* **2013**, *7*, 2898.
[5] B. Sipos, A. F. Kusmartseva, A. Akrap, H. Berger, L. Forro, E. Tutis, *Nat. Mater.* **2008**, *7*, 960.
[6] R. Thomson, B. Burk, A. Zettl, J. Clarke, *Phys. Rev. B: Condens. Matter* **1994**, *49*, 16899.
[7] L. Stojchevska, I. Vaskivskyi, T. Mertelj, P. Kusar, D. Svetin, S. Brazovskii, D. Mihailovic, *Science* **2014**, *344*, 177.
[8] B. Radisavljevic, A. Radenovic, J. Brivio, V. Giacometti, A. Kis, *Nat. Nanotechnol.* **2011**, *6*, 147.
[9] B. Radisavljevic, M. B. Whitwick, A. Kis, *ACS Nano* **2011**, *5*, 9934.
[10] R. F. Frindt, A. D. Yoffe, *Proc. R. Soc. London A* **1962**, *273*, 69.
[11] F. Mak, C. Lee, J. Hone, J. Shan, T. F. Heinz, *Phys. Rev. Lett.* **2010**, *105*, 136805.
[12] A. Splendiani, L. Sun, Y. Zhang, T. Li, J. Kim, C.-Y. Chim, G. Galli, F. Wang, *Nano Lett.* **2010**, *10*, 1271.
[13] B. L. Evans, P. A. Young, *Proc. Phys. Soc.* **1967**, *91*, 475.
[14] A. Ramasubramaniam, *Phys. Rev. B: Condens. Matter* **2012**, *86*, 115409.
[15] T. Cheiwchanchamnangij, W. R. L. Lambrecht, *Phys. Rev. B: Condens. Matter* **2012**, *85*, 205302.
[16] Z. Ye, T. Cao, K. O'Brien, H. Zhu, X. Yin, Y. Wang, S. G. Louie, X. Zhang, *Nature* **2014**, *513*, 214.
[17] M. Fontana, T. Deppe, A. K. Boyd, M. Rinzan, A. Y. Liu, M. Paranjape, P. Barbara, *Sci. Rep.* **2013**, *3*, 1634.
[18] O. Lopez-Sanchez, D. Lembke, M. Kayci, A. Radenovic, A. Kis, *Nat. Nanotechnol.* **2013**, *8*, 497.

[19] K. F. Mak, K. He, C. Lee, G. H. Lee, J. Hone, T. F. Heinz, J. Shan, *Nat. Mater.* **2012**, *12*, 207.
[20] S. Mouri, Y. Miyauchi, K. Matsuda, *Nano Lett.* **2013**, *13*, 5944.
[21] N. Scheuschner, O. Ochedowski, A. M. Kaulitz, R. Gillen, M. Schleberger, J. Maultzsch, *Phys. Rev. B: Condens. Matter* **2014**, *89*, 125406.
[22] N. Dean, J. C. Petersen, D. Fausti, R. I. Tobey, S. Kaiser, L. V. Gasparov, H. Berger, A. Cavalleri, *Phys. Rev. Lett.* **2011**, *106*, 016401.
[23] R. Osterbacka, C. An, X. Jiang, Z. Vardeny, *Science* **2000**, *287*, 839.
[24] V. I. Klimov, S. A. Ivanov, J. Nanda, M. Achermann, I. Bezel, J. A. McGuire, A. Piryatinski, *Nature* **2007**, *447*, 441.
[25] J. Cabanillas-Gonzalez, T. Virgili, A. Gambetta, G. Lanzani, T. D. Anthopoulos, D. M. de Leeuw, *Phys. Rev. Lett.* **2006**, *96*, 106601.
[26] C. Gadermaier, E. Menna, M. Meneghetti, W. J. Kennedy, Z. V. Vardeny, G. Lanzani, *Nano Lett.* **2006**, *6*, 301.
[27] R. Gatensby, N. McEvoy, K. Lee, T. Hallam, N. C. Berner, E. Rezvani, S. Winter, M. O'Brian, G. S. Duesberg, *Appl. Surf. Sci.* **2014**, *297*, 139.
[28] C. Lee, H. Yan, L. E. Brus, T. F. Heinz, J. Hone, S. Ryu, *ACS Nano* **2010**, *4*, 2695.
[29] H. Li, Q. Zhang, C. C. R. Yap, B. K. Tay, T. H. T. Edwin, A. Olivier, D. Baillargeat, *Adv. Funct. Mater.* **2012**, *22*, 1385.
[30] H. Shi, R. Yan, S. Bertolazzi, J. Brivio, G. Bao, A. Kis, D. Jena, H. G. Xing, L. Huang, *ACS Nano* **2013**, *7*, 1072.
[31] C. Mai, A. Barrette, Y. Yu, Y. G. Semenov, K. W. Kim, L. Cao, K. Gundogdu, *Nano Lett.* **2014**, *14*, 202.
[32] D. Sercombe, S. Schwarz, O. Del Pozo-Zamudio, F. Liu, B. J. Robinson, E. A. Chekhovich, I. I. Tartakovskii, O. Kolosov, A. I. Tartakovskii, *Sci. Rep.* **2013**, *3*, 3489.
[33] G. Plechinger, F.-X. Schrettenbrunner, J. Eroms, D. Weiss, C. Schuller, T. Korn, *Phys. Status Solidi RRL* **2012**, *6*, 126.
[34] H. R. Gutierrez, N. Perea-López, A. L. Elías, A. Berkdemir, B. Wang, R. Lv, F. López-Urías, V. Crespi, H. Terrones, M. Terrones, *Nano Lett.* **2013**, *13*, 3447.
[35] L. Yadgarov, C. L. Choi, A. Sedova, A. Cohen, R. Rosentsveig, O. Bar-Elli, D. Oron, H. Dai, R. Tenne, *ACS Nano* **2014**, *8*, 3575.
[36] G. Soavi, F. Scotognella, D. Brida, T. Hefner, F. Späth, M. R. Antognazza, T. Hertel, G. Lanzani, G. Cerullo, *J. Phys. Chem. C* **2013**, *117*, 10849.
[37] S. Sim, J. Park, J.- G. Song, C. In, Y.-S. Lee, H. Kim, H. Choi, *Phys. Rev. B: Condens. Matter* **2013**, *88*, 075434.
[38] G. Tränkle, E. Lach, A. Forchel, F. Scholz, C. Ell, H. Haug, G. Weimann, G. Griffiths, H. Kroemer, S. Subbanna, *Phys. Rev. B: Condens. Matter* **1987**, *36*, 6712.
[39] Q. Wang, S. Ge, X. Li, J. Qiu, Y. Ji, J. Feng, D. Sun, *ACS Nano* **2013**, *7*, 11087.
[40] M. M. Ugeda, A. J. Bradley, S.-F. Shi, F. H. da Jornada, Y. Zhang, D. Y. Qiu, W. Ruan, S.-K. Mo, Z. Hussain, Z.-X. Shen, F. Wang, S. G. Louie, M. F. Crommie, *Nat. Mater.* **2014**, *13*, 1091.
[41] Q. Y. Ouyang, H. L. Yu, K. Zhang, Y. J. Chen, *J. Mater. Chem. C* **2014**, *2*, 6319.
[42] D. Kozawa, R. Kumar, A. Carvalho, K. K. Amara, W. Zhao, S. Wang, M. Toh, R. M. Ribeiro, A. H. Castro Neto, K. Matsuda, G. Eda, *Nat. Commun.* **2014**, *5*, 4543.
[43] S. Schmitt-Rink, D. S. Chemla, D. A. B. Miller, *Adv. Phys.* **1989**, *38*, 89.
[44] M. Yan, L. J. Rothberg, E. W. Kwock, T. M. Miller, *Phys. Rev. Lett.* **1995**, *75*, 1992.
[45] C. Manzoni, A. Gambetta, E. Menna, M. Meneghetti, G. Lanzani, G. Cerullo, *Phys. Rev. Lett.* **2005**, *94*, 207401.
[46] C. Gadermaier, G. Cerullo, G. Sansone, G. Leising, U. Scherf, G. Lanzani, *Phys. Rev. Lett.* **2002**, *89*, 117402.
[47] J. Noolandi, K. M. Hong, *J. Chem. Phys.* **1979**, *70*, 3230.
[48] V. I. Arkhipov, E. V. Emilianova, H. Bassler, *Phys. Rev. Lett.* **1999**, *82*, 1321.
[49] A. Leitenstorfer, C. Furst, A. Laubereau, W. Kaiser, G. Trankle, G. Weimann, *Phys. Rev. Lett.* **1996**, *76*, 1545.
[50] D. Sun, Z.-K. Wu, C. Divin, X. Li, C. Berger, W. A. de Heer, P. N. First, T. B. Norris, *Phys. Rev. Lett.* **2008**, *101*, 157402.
[51] C. Gadermaier, V. V. Kabanov, A. S. Alexandrov, L. Stojchevska, T. Mertelj, C. Manzoni, G. Cerullo, N. D. Zhigadlo, J. Karpinski, Y. Q. Cai, X. Yao, Y. Toda, M. Oda, S. Sugai, D. Mihailovic, *Phys. Rev. X* **2014**, *4*, 011056.
[52] L. Dhar, J. A. Roger, K. A. Nelson, *Chem. Rev.* **1994**, *94*, 157.
[53] T. Ichibayashi, S. Tanaka, J. Kanasaki, K. Tanimura, T. Fauster, *Phys. Rev. B: Condens. Matter* **2011**, *84*, 235210.
[54] T. Korn, S. Heydrich, M. Hirmer, J. Schmutzler, C. Schüller, *Appl. Phys. Lett.* **2011**, *99*, 102109.
[55] G. Wang, X. Marie, L. Bouet, M. Vidal, A. Balocchi, T. Amand, D. Lagarde, B. Urbaszek, *Appl. Phys. Lett.* **2014**, *105*, 182105.
[56] C. Mai, A. Barrette, Y. F. Yu, Y. G. Semenov, K. W. Kim, L. Y. Cao, K. Gundogdu, *Nano Lett.* **2014**, *14*, 202.
[57] D. Lagarde, L. Bouet, X. Marie, C. R. Zhu, B. L. Liu, T. Amand, P. H. Tan, B. Urabaszek, *Phys. Rev. Lett.* **2014**, *114*, 047401.
[58] M. J. Assael, S. Botsios, J. Gialou, I. N. Metaxa, *Int. J. Thermophys.* **2005**, *26*, 1595.
[59] Q. C. Sun, L. Yadgarov, R. Rosentsveig, G. Seifert, R. Tenne, J. L. Musfeldt, *ACS Nano* **2013**, *7*, 3506.
[60] A.Pospischil, M. M. Furchi, T. Mueller, *Nat. Nanotechnol.* **2014**, *9*, 257.
[61] B. W. H. Bauger, H. O. H. Churchill, Y. F. Yang, P. Jarillo-Herrero, *Nat. Nanotechnol.* **2014**, *9*, 262.
[62] L. Britnell, R. M. Ribeiro, A. Eckmann, R. Jalil, B. D. Belle, A. Mishchenko, Y.-J. Kim, R. V. Gorbachev, T. Georgiou, S. V. Morozov, A. N. Grigorenko, A. K. Geim, C. Casiraghi, A. H. Castro Neto, K. S. Novoselov, *Science* **2013**, *340*, 1311.
[63] C.-H. Lee, G.-H. Lee, A. M. van der Zande, W. Chen, Y. Li, M. Han, X. Cui, G. Arefe, C. Nuckolls, T. F. Heinz, J. Guo, J. Hone, P. Kim, *Nat. Nanotechnol.* **2014**, *9*, 676.
[64] X. Hong, J. Kim, S.-F. Shi, Y. Zhang, C. Jin, Y. Sun, S. Tongay, J. Wu, Y. Zhang, F. Wang, *Nat. Nanotechnol.* **2014**, *9*, 682.